Robotics and Autonomous Systems 63 (2015) 253–267

Contents lists available at ScienceDirect

Robotics and Autonomous Systems

journal homepage: www.elsevier.com/locate/robot

A novel model for assessing sliding mechanics and tactile sensation of human-like fingertips during slip action

Van Anh Ho *, Shinichi Hirai

Soft Robotics Laboratory, Ritsumeikan University, 1-1-1 Noji-Higashi, Kusatsu City, Shiga Prefecture, 525-8577, Japan

HIGHLIGHTS

- We have extracted human fingertip structure using MR images.
- We have modeled the inhomogeneous human fingertip with proposed Beam Bundle Model as a platform that reduces remarkably calculation time.
- Investigating sliding mechanics of the model, such as friction, and especially the localized displacement phenomenon during pre-slide phase.
- Verifying the model with an artificial human-like fingertip and a fine experimental setup.
- Pointing out the role of localized displacement phenomenon in assessing tactile sensing perception and its application in robotics.

ARTICLE INFO

Article history:
Available online 15 October 2014

Keywords:
Human fingertip modeling
Beam bundle model
Haptics
Localized slippage
Slip detection

ABSTRACT

This paper presents a model for displaying friction and localized stick/slip of sliding inhomogeneous human-like fingertips, to understand how slippage occurs and its role in assessing tactile sensing mechanics. In the absence of friction, the fingertip slides, as on an ice surface, in the virtual world of haptic interfaces. Slippage of fingertip at very low velocity can reflect micro stick/slip on a contact area, which is challenging to represent in any friction model. To overcome these drawbacks, we propose that a Beam Bundle Model (BBM) can be used to model a human fingertip during pushing and sliding actions, especially during stick-to-slip transition. To construct its three-dimensional, non-homogeneous structure, we obtained a sequential series of magnetic resonance images, showing consecutive cross-sectional layers of a fingertip with distribution of skin, tissue, bone, and nail. Simulation results showed that this model could generate not only normal force distribution caused by pushing, but also response of friction during stick-to-slip transition. Secondly, and more interestingly, the model dynamically produced localized displacement phenomena on the contact area during stick-to-slip phase, indicating how slippage enlarges the contact area prior to total slippage of the fingertip. These findings may better assess the sliding processes of human fingertips, and how and when slippage occurs on the contact surface. This model may be a useful platform for studying tactile perception of fingertips.

1. Introduction

Increase in the use of tablet devices, which involve the touching/sliding of fingertips on their surfaces, requires understanding of the characteristics of touching by human fingers, aiming at enhanced dexterity during human–machine interactions. Tactile perception is considered important for both humans and robots, enabling acquisition of information from the outside world, especially the characteristics of a grasped object for stable/dexterous manipulation. Research on tactile perception in robotics for over 30 years has focused mainly on mimicking the action of human fingertips, by arranging the shape, function, structure and distribution of mechanoreceptors [1]. In the virtual world of a haptic system, successful tactile exploration has been found to require creation of a significant *sense* of realness by the user [2]. Especially for soft fingertips moving at low velocity from a starting sliding state, there are localized/partial movements of contacting points, called a pre-slide regime [3]. Several friction models [4] are successful at representing the pre-slide phase of soft objects as an increase of friction force over movement of the object. Nonetheless, the details of partial movements on a contacting area during the stick phase are impossible to determine.

In this research, we attempted to use a *Beam Bundle Model* (BBM) to model a human fingertip. In order to create a structure

* Corresponding author.
E-mail addresses: hoanhvan@gmail.com (V.A. Ho), hirai@se.ritsumei.ac.jp (S. Hirai).

http://dx.doi.org/10.1016/j.robot.2014.09.009
0921-8890/

as close as possible to a human fingertip in a virtual environment, we utilized magnetic resonant images (MRI) of a volunteer's fingertip to construct a mathematical model of the structure of a fingertip. We first characterized the pre-sliding regime on a real human finger to determine the most important factors for haptic display. We afterward simulated the model, successfully representing localized displacements, or skin local stretch, during the pre-slide phase of the fingertip, which is considered crucial in assessing stick/slip events on a contacted surface. This work can be utilized not only in haptic sensation, but also in the development of sensors for detection of slippage.

2. Related work

2.1. Fingertip modeling in robotics

Modeling bio-mimetically structured fingertips started with a homogeneous soft fingertip model, in which fingertips possess simple geometrical shapes, such as cylindrical or hemispherical shapes. Maeno et al. [5] proposed a linear FEM model of a simple fingertip, considering the positions of strain gauges, to investigate the responses of these sensing systems during grasping of an object. To verify power-law theory in material mechanics, Xydas et al. [6] utilized nonlinear FE analysis to study contact mechanics of a hemispheric fingertip, focusing primarily on normal contact that causes a pressure distribution profile over the contact zone. Ho et al. [3] recently introduced a three-dimensional model of an elastomer hemispherical fingertip in a context of sliding motion to optimize location of a micro sensor that efficiently senses multiple states of contact with the outside environment. Uniform models, however, are insufficient for further understanding of the functions of human fingertips, to mimic in robotic fingertips. Thus, nonhomogeneous models with multiple structures, such as tissue, bone, and nail, have been developed. For example, an FE-based two-dimensional model of a soft fingertip with a simple structure of bone inside has been proposed [7]. Simulation results showed that the appearance of bone in many configurations contributed significantly to force distribution, as well as to responses from mechanoreceptors. As an extension of this research [8], a three-dimensional FE model of human and monkey fingertips, with five layers of epidermis, dermis, and bone, was developed to investigate the roles of the epidermis, as well as the stiffness of other layers, in representing a line load on the fingertip. Although this model perfectly fitted the experimental data, calculation times are long. Moreover, this model ignored friction, as well as dynamic responses during sliding motions. A more complicated model of a human fingertip with accurate geometries generated from computed tomography (CT) images was proposed [9] to study deformation of the fingertip on a flat plate. More recently, Tada [10] constructed a three-dimensional FE model of 50 subjects' fingertips, based on MRI, and showed variations in contact pressure among subjects. All of the above research, however, addressed static models that predict stress–strain when making contact, but could not simulate dynamic changes in stress–strain over time.

2.2. Modeling of a fingertip's sliding motion

Determination of sliding action is crucial for a fingertip during grasping or manipulation, as well as for tactile perception, in which a human/robot must slide a finger along a surface, so that mechanoreceptors underneath the skin can determine the textural characteristics of the surface, which are decoded by the brain/controller. In addressing sliding motion, Kao and Cutkosky [11] built a closed-form for modeling manipulation with sliding fingers. However, this research was limited to quasi-static simulation and homogeneous fingertips, and could not assess details of slippage on the contact area. Konyo et al. [12] investigated human fingertip under vibro tactile stimuli to represent force in a haptic display system. A dynamic model of a human fingertip was proposed to study stick/slip events on the contact surface in the presence of external high-frequency stimuli. This model consisted of a mass connected to a spring and a damper arranged in parallel, making it insufficient to model the complicated structure of human fingertip. Recently, a complete FE model of a human fingertip with dynamic approach was proposed [13]. However, sliding action has not yet been addressed fully, since friction force has not been included. Moreover, considerable time is required to implement a simulation trial of this model, making this model impossible to apply in a real time haptic system. Recently, Nahvi et al. [2] introduced a friction display system for a virtual environment, using a simplified model of a virtual spring during transition from slip to stick, and vice versa. While this model can determine the characteristics of a human fingertip, such as switching between stick and slip and oscillation in slip phase, it cannot determine how partial slippage occurs on a contact area during stick phase, a determination crucial in assessing slip perception.

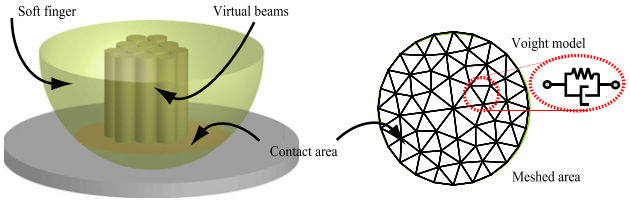

Fig. 1. Beam Bundle Model.

2.3. Model of a robotic soft fingertip

Previously, we proposed a model to simulate the sliding motion of cylindrical and hemispheric soft fingertips. In this model, the soft fingertip was elastic and homogeneous with a pre-determined geometric shape. This model was a hybrid of a discrete model and a finite element model as shown in Fig. 1. First, to model the deformation of the fingertip under normal and tangential loads, we filled in the volume of the fingertip with *virtual* elastic beams, which can be compressed and bent. Thus, deformation of the fingertip was calculated based on the deformation of all beams. Second, the contact area was meshed with a viscoelastic model, according to finite element theory. Free ends of beams were placed at nodes on the contact area, such that the mutual interactions among beams were solely on the contact surface. Detailed derivation of motion equations were illustrated [14]. Using this model, we were able to simulate sliding motion at a given speed, and observe responses of normal and frictional forces. Moreover, simulation produced localized displacement phenomena during the pre-slide phase, helping us to assess how and when slippage occurred on the contact surface. This is considered important in understanding the slippage of a soft object, as well as being crucial to tactile sensation. Application of this tool to model human fingertips is described in the following sections.

3. Frictional characteristics of human fingertips

Current robotic fingertips differ from human fingertips in structure and function. Human fingertips consist of three main layers: the epidermis, dermis, and bone. In addition, human fingertips contain a high density of blood vessels and lymphatics, forming a network in the tissue, as well as a mechanoreceptor system. Thus, human fingertips are complicated, inhomogeneous structures, in which soft tissue deforms and recovers continuously, depending

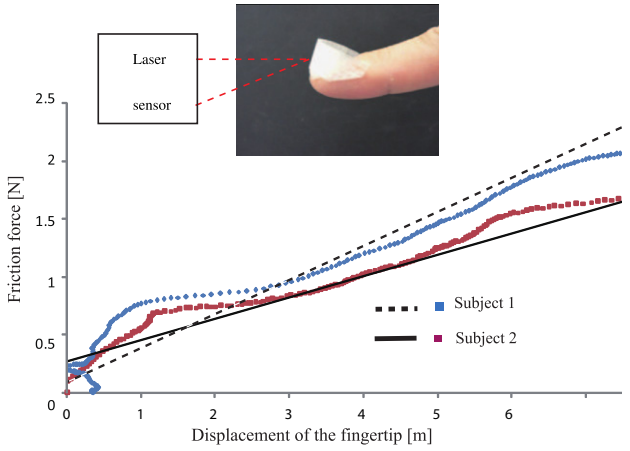

Fig. 2. Linear relation between friction and movement of the fingertip.

on external load. Thus, it is necessary to characterize a human fingertip's slip action to assess the predominant type of phenomena and to simulate real conditions into any proposed model. To characterize human fingertips, subjects were asked to push and slide their fingertips on a rigid, transparent surface. Translational movement of the finger was tracked by a laser range sensor (LB-01, Keyence, Japan), with a resolution of 0.1 mm, while three components of force applied to the surface were recorded by a 3-dof loadcell (USL6-H5-50N-C, Tekgihan, Japan). Moreover, a pressure distribution sensor (ISCAN-50, Nitta, Japan) was used to assess normal force distribution when pushing the finger, and a high speed camera (Photonfocus MV1-D1600, Switzerland) was used to assess *detailed* deformations of the contact area of the fingertip during sliding. A display showing components of force and pressure distribution allowed subjects to adjust applied loads as required. As mentioned in Section 1, we focused on pre-slide characteristics of human fingertips.

Several friction models have mentioned the *spring-like* relationship between frictional forces and displacement of objects, especially soft objects, during the stick phase. We investigated these characteristics of human fingertips by asking subjects to start to slide their fingers slowly enough so that their movement could be captured by a laser displacement sensor, while loadcell measures frictional force. A light-weight shield was attached to the nail of each fingertip to correctly reflect the laser beam from the displacement sensor (see the inset in Fig. 2). The subject could change angle of inclination or depth of contact. Plots shown in Fig. 2 show a roughly linear relationship between frictional force and displacement of the fingertip, indicating a stick phase prior to gross sliding of the fingertip; when the fingertip gives way, the contact area still sticks, causing friction to increase [4]. This phenomenon in human fingertips should be included in any proposed model. The linear spring model [2] does not sufficiently represent this phenomenon, since the friction of human fingertips experience high hysteresis during sliding.

3.1. Localized displacement during stick phase

Much experimental research has assessed partial movements on the contact area during the pre-slide phase (*i.e.* stick phase as aforementioned) of soft robotic fingertips [11,14]. This phenomenon also likely occurs on human fingertips, due to their soft dermis and curved shape. We attempted to verify this phenomenon by marking black dots onto the skin of subjects' fingertips, and monitoring the movement of these dots with a high speed camera [15] when subjects slid their fingers, starting from rest, in different directions, attempting not to change velocity or normal force. Fig. 3 shows the tracking results of dots along the contact area, with dot movements indicated by white bars during the pre-slide phase. This experiment showed *localized displacements* of contacting dots in the stick phase, starting from the boundary areas of the contact pad and propagating to the inner area, such that the slip phase occurs only when these partial movements dominate throughout the contact pad. Similarly, partial movement propagation differed when the direction of slide changed. Similar results were also reported recently [10,16]. To date, no analytical model could tackle this issue in its closed form, since the transition between stick–slip states at each contact point has an inherent discontinuity. Thus, a simulation model is necessary in which generalized displacements of contact points can be derived during stick–slip transition.

3.2. Relation of contact angle and contact area

Some contact models [17] and power modes [6] deal with contact area of soft objects during normal contact. To date, however, no model has addressed the role of the contact area during relative sliding. In this experiment, subjects were asked to change contact depth, thus varying contact area, during sliding. Since normal force is altered by change in contact depth, the resulting friction changes accordingly. The most interesting results were observed during trials in which subjects attempted to maintain normal force unchanged, then rotated their fingers to change the inclination of contact angle. We observed a decreasing linear relationship between contact area and contact angle (Fig. 4). This differed greatly from results obtained using typical robotic soft fingertips, such as cylindrical or hemispherical fingertips, in which the contact area remained unchanged during rotation [3]. These issues must therefore be considered to fully describe the inherent characteristics of human fingertips in the model.

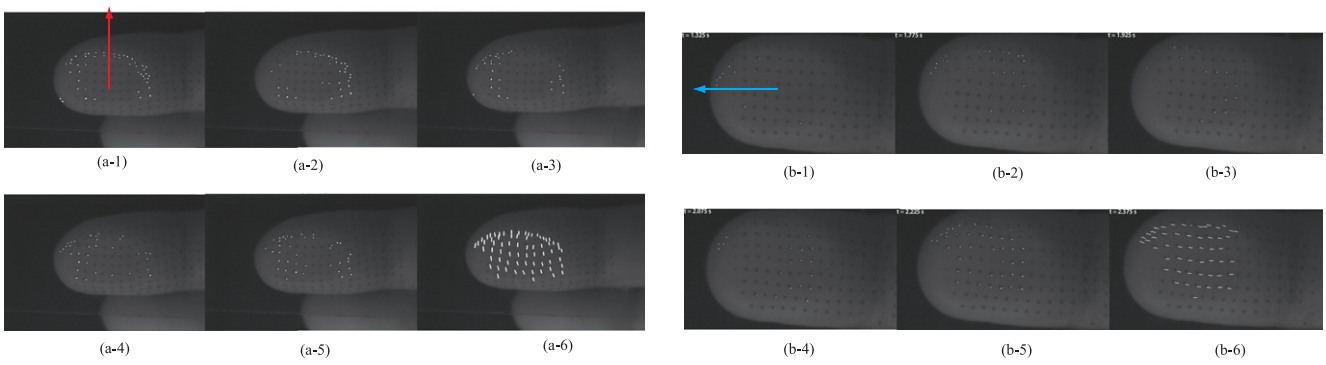

(a) When the fingertip slides laterally (indicated by the red arrow).

(b) When the fingertip slides forward (indicated by the blue arrow).

Fig. 3. Movements on the contact area during the stick phase. White dots/bars indicated the slipped points on the contact pad. (For interpretation of the references to color in this figure legend, the reader is referred to the web version of this article.)

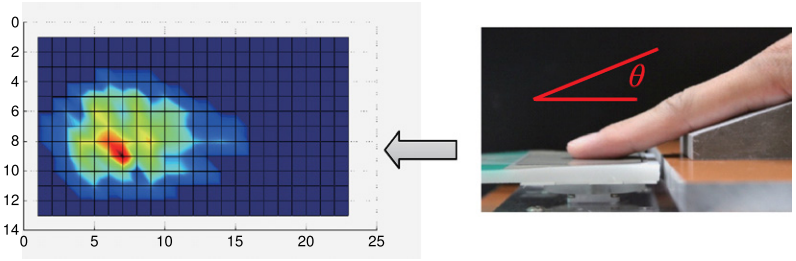

(a) Contact area and normal force distribution obtained from tactile sensor.

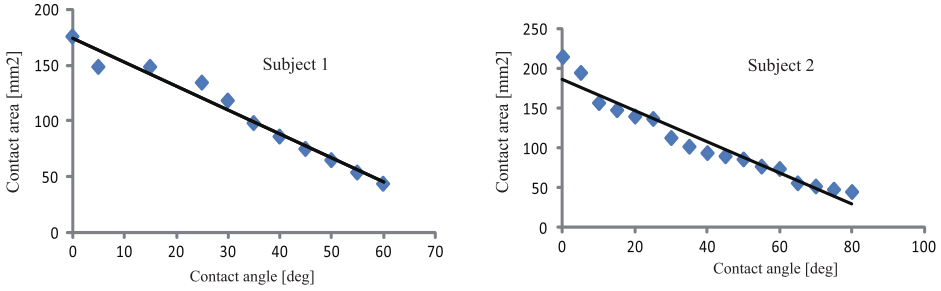

(b) Relation between contact area and inclination contact angle θ.

Fig. 4. Linear decrease of contact area over change of inclination contact angle during rotation action.

4. Beam Bundle Model of human fingertip

4.1. Construction of human fingertip using MR images

A 3 T (3T) MRI system, SIGNA HDXT (GE Healthcare, Waukesha, WI) was used to accurately measure the 3D internal and external geometries of a human fingertip. Cross-sectional MR images were obtained of an index finger of a 25-year-old male with no history of finger disease. A set of 32 images with 120×120 mm^2 field of view (FOV), 1.2 mm slice thickness and 512×512 matrices (pixel size of $0.23 \times 0.23 \times 1.2$ mm^3) were acquired using a 3D fast gradient echo (fgre) sequence with 9.8 ms repetition time (TR), 4.2 ms echo time (TE) and 30 flip angle. The consecutive cross-sectional layers of these images were utilized to determine fingertip volume. In each image, we observed the distribution and position of skin, tissue, bone, and nail, as illustrated in Fig. 5.

To introduce the BBM to human fingertips, it was necessary to assess the exact distribution of inner layers, allowing virtual beams to be filled in properly. Image processing functions in OpenCV were used to assess the boundaries of skin and bone, and the position of the nail. Since MR signals are mainly derived from protons of water molecules in body tissues, we were not able to assess the shape of the nail, which is dry, but were able to assess only the boundary. Each boundary was formed by a group of points that were afterward interpolated into a curve (see Fig. 6(a)). Thus, for each image, we were able to collect four fitted curves, including those for the skin, lower bone, upper bone, and nail (Fig. 6(a)). By repeating this process on all images, a three-dimensional geometrical shape of the fingertip could be constructed for introduction of BBM.

4.2. Application of BBM to a human fingertip

As mentioned in Section 4, the volume of the fingertip had to be filled in by virtual beams, after assessing the distribution of inner structures, such as soft tissue and bone. For each layer of the image, using the fitted curves mentioned above, we were able to attach virtual beams to the tissue volume, so that a fixed end of one beam was pinned into a rigid structure, such as nail or bone, while the other end of the beam was present on the boundary of the skin.

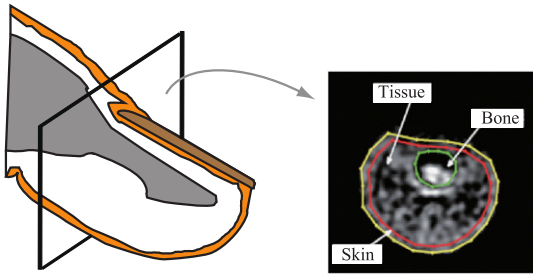

Fig. 5. MR images of consecutive cross-sectional layers of a human fingertip, showing the distribution of skin, phalanx, and nail.

Each virtual beam was cylindrical in shape with geometrical properties, such as height, based on fitted curves for nail, bone, and skin. Since layers of MR images have a pitch of 1.2 mm along the volume of the fingertip, and since we intended to fit the beams to the volume of the fingertip, each beam had a cross-sectional diameter of 1.2 mm, making the distance between the basic axes of two neighboring beams 1.2 mm. After filling in the virtual beams (Fig. 6(b)), we observed three groups of beams, those attached to nail and skin (N–S), bone and skin (B–S), and nail and bone (N–B). This model assumed that, during sliding motion, which includes both pushing and sliding actions, nail and bone are not deformed. Thus, beams in group N–B do not deform during action of the fingertip model, with group N–S and B–S beams contributing to the deformation of fingertip volume. By filling in beams into the volume of the fingertip, the deformation of tissue in the fingertip would be represented or replaced by deformations of virtual beams, drastically reducing calculation time compared with FE analysis.

Suppose that a fingertip was pushed vertically onto a rigid flat surface, resulting in a set of contact boundary points on skin. The contact area could then be meshed utilizing finite element analysis, covering the contact area with a set of triangles (Fig. 7(a)). The stress–strain relationship of each triangle can be represented by a Kelvin–Voigt element, which includes a spring and a damper connected in parallel (Fig. 7(b)). Each triangle has three nodes attached to the free ends of three N–S and/or B–S beams (see Fig. 7(c)). Beams can partly cover or be superpositioned on each

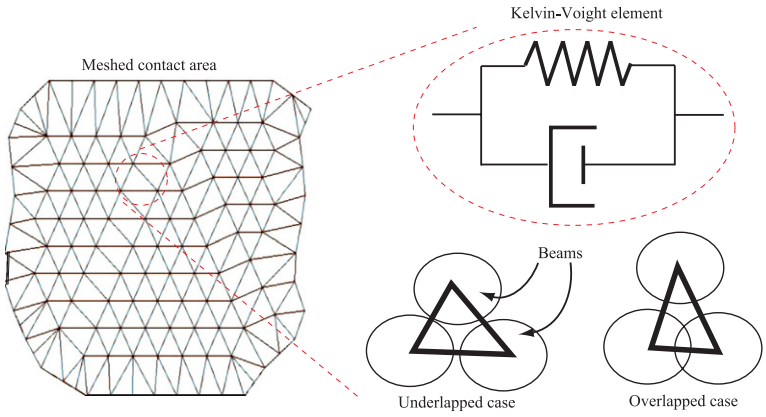

Fig. 6. Structure of human fingertip from MRI.

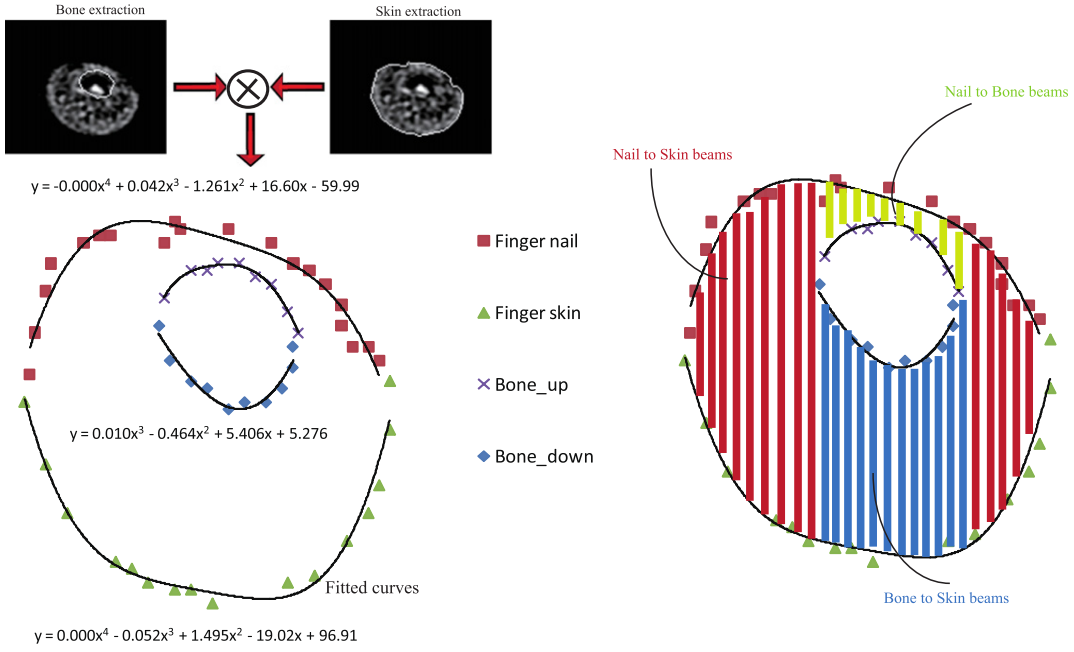

(a) Structure extraction

(b) Groups of virtual beams inside the fingertip

Fig. 7. Meshed contact area.

triangle, with the former occurring more frequently, making the coverage ratio of the entire contact area less than 100%. Coverage depends on how coarse or fine the contact area is meshed, with the maximum ratio reached with minimal superposition being 96%. Thus, coverage ratio can be altered by varying the geometric shape of the beams to adapt to specific simulations. Beams are therefore constrained on the contact area of the skin, with the movement of the free-ends of the beams helpful in assessing stick/slip events on the contact area during sliding motion. We have called this model the Beam Bundle Model (BBM).

4.3. Derivation of motion equation

This section summarizes several important equations that describe the dynamic movement of a fingertip, as well as the contact area. Motion equations of an entire fingertip can be derived similar to hemispheric phase [14]. Suppose that a fingertip was pushed vertically onto a flat surface, then slid horizontally at constant speed. Virtual beams are then deformed, with both normal and bending deformation. Several assumptions have been made to simplify calculations:

1. Interactions between neighboring beams only occur among their free ends *on* the contact zone.
2. Only beams whose free ends are acting on the contact surface are considered. Beams outside the contact surface are deemed irrelevant to the sliding motion of the fingertip.
3. Nail and bone (phalanx) are completely rigid and do not deform during sliding motion of the fingertip.
4. The area of the nail is always larger than the contact area.

The first and the second assumptions are important in drastically reducing calculation costs. Although the tissue volume of a fingertip is uniformly deformed, skin on the contact area stretches differently in various locations, making the first assumption acceptable. Since superposition of beams is small and irrelevant to the precision of the model, beams deformed by pushing action do not affect beams positioned outside the boundary of the contact area; thus, the second assumption is sufficient for modeling deformation of an entire fingertip. Young's moduli of tissue, skin, and bone of a human fingertip are shown in Table 1. Young's modulus of bone is much larger than moduli of tissue and skin, while the nail is considered to be undeformable (or rigid). This makes the third

Table 1
Physical parameters for the human fingertip [13].

	Tissue	Skin	Bone
E (Pa)	3.4×10^4	1.36×10^5	1.5×10^9
c (Pa s)	Not used	10	Not used

assumption also acceptable for calculations without degrading the precision of the model. This assumption also allows us to neglect deformation of beams in group N–B, since they are positioned between two undeformable layers, nail and bone. Thus, we only consider the deformation of the two remaining beam groups, N–S and B–S (see Fig. 6(b)). The last assumption is a reality, since most human fingertips possess nails that cover almost the entire upper part of the fingertip. This allows the elimination of beams on the contact area that do not contact bone or nail, but are pinned to the skin. Using these assumptions, we were able to formulate force calculation and motion equations. First, for normal force, each beam that makes contact with the flat surface shows a deformation d_n^i, which is calculated based on the geometric relative position between the fingertip and the surface. Thus, the normal force exerted on each contacting beam can be calculated as:

$$f_n^i = k^i d_n^i = E \frac{\pi {r_o^i}^2}{l_o^i} d_n^i, \tag{1}$$

where k^i is stiffness, E is Young's modulus, l_o^i is natural length, and r_o^i is natural cross-sectional radius. Upon activation of the external tangential force F_t, the fingertip has not yet been slid. The contact surface still sticks to the plane, causing the fingertip to deform. At this time, all contacting beams are bent at their free ends with the same bending strain δs, calculated as in [18]:

$$\delta s = \frac{3\mu F_n}{16R} \frac{2-\nu}{G} \{1 - (1-\Phi)^{2/3}\}, \tag{2}$$

where F_t, F_n are tangential and normal forces, respectively, $\Phi = F_t/\mu F_n$ is the tangential force coefficient, R is the radius of the fingertip, μ is the coefficient of friction, ν is Poisson's ratio, and G is shear elasticity's modulus. By assessing the bending strain in Eq. (2), the bending force f_b^i acting on the free end of the cantilever, with length l^i and radius of cross-sectional area r^i, can be calculated as:

$$f_b^i = b^i \delta s = \frac{3EI}{(l^i)^3} \delta s = \frac{3E\pi (r^i)^4}{(l^i)^3} \delta s. \tag{3}$$

FE-based meshed contact areas have visco-elastic forces at each contact node, calculated based on the geometric characteristic of the node in the context of interaction with neighboring nodes:

$$\mathbf{F}_{\text{ve}} = (\lambda^{\text{ela}} \mathbf{J}_\lambda + \mu^{\text{ela}} \mathbf{J}_\mu)\mathbf{u}_N + (\lambda^{\text{vis}} \mathbf{J}_\lambda + \mu^{\text{vis}} \mathbf{J}_\mu)\mathbf{v}_N, \tag{4}$$

and:

$$\mathbf{v}_N = \dot{\mathbf{u}}_N, \tag{5}$$

where $\mathbf{u}_N$ and $\mathbf{v}_N$ are generalized displacements and velocities of nodes. The above equation is equivalent to:

$$\mathbf{f}_{\text{ve}} = \mathbf{K}_{\text{ela}} \mathbf{u}_N + \mathbf{K}_{\text{vis}} \dot{\mathbf{u}}_N, \tag{6}$$

where λ^{ela}, and μ^{ela} as elastic Lame's constants; λ^{vis}, and μ^{vis} as viscous Lame's constants. Connection matrices can be described as $\mathbf{J}_\lambda$, and $\mathbf{J}_\mu$ which can be obtained by synthesizing partial connection matrices of triangles. We also introduced friction law into each node on the contact surface. Its value changed based on its contact state: stick or slip, and was calculated correspondingly. For the stick case:

$$\mathbf{f}_{\text{ve}}^i + \mathbf{f}_b^i < \mu \mathbf{f}_n^i \Rightarrow \mathbf{A}^i = \mathbf{A}_1^i \Rightarrow \mathbf{f}_{fr}^i = \mathbf{f}_{\text{ve}}^i + \mathbf{f}_b^i, \tag{7}$$

Table 2
Simulation parameters.

Sliding speed (mm/s)	Friction coefficient	Direction of slide
From 2.0 to 5.0	From 0.6 to 2.0	$X+, X-, Y+, Y-$

while in the slip case:

$$\mathbf{f}_{\text{ve}}^i + \mathbf{f}_b^i \geq \mu \mathbf{f}_n^i \Rightarrow \mathbf{A}^i = \mathbf{A}_0^i \Rightarrow \mathbf{f}_{fr}^i = \mu \mathbf{f}_n^i, \tag{8}$$

where $\mathbf{A}^i$ is a 2×2 matrix describing the constraint on the ith node, in which $\mathbf{A}_1^i$ is the 2×2 identical matrix, while $\mathbf{A}_0^i$ is the 2×2 null matrix. Finally, using a Lagrangian formula and a Constraint Stabilization Method (CSM), we were able to construct motion equations for all contacting nodes on the contact area:

$$\begin{bmatrix} \mathbf{I} & \mathbf{0} & \mathbf{0} \\ \mathbf{0} & \mathbf{M} & -\mathbf{A} \\ \mathbf{0} & -\mathbf{A}^T & \mathbf{0} \end{bmatrix} \begin{bmatrix} \dot{\mathbf{u}}_N \\ \dot{\mathbf{v}}_N \\ \boldsymbol{\lambda} \end{bmatrix} = \begin{bmatrix} \mathbf{v}_N \\ -\mathbf{K}_{\text{ela}} \mathbf{u}_N - \mathbf{K}_{\text{vis}} \mathbf{v}_N + \mathbf{F} \\ \mathbf{A}^T (2\omega \mathbf{v}_N + \omega^2 \mathbf{u}_N) \end{bmatrix}, \tag{9}$$

where $\boldsymbol{\lambda}$ is the Lagrangian multiplier matrix, $\mathbf{M}$ is the inertia matrix of the contact pad, $\mathbf{A}$ is constraint matrix, and ω is the angular velocity determined using CSM. This equation is linear and solvable since the matrix is regular, indicating that $\dot{\mathbf{u}}_N$, and $\dot{\mathbf{v}}_N$, the displacements and velocities of the contacting nodes, respectively, can be calculated. Details of this derivation can be seen in the previous paper [14].

5. Simulation

In this simulation, the fingertip was vertically pushed at a predetermined contact depth, resulting in tangential movement at constant velocity. Parameters used for simulation are summarized in Tables 1 and 2.

5.1. Force-related results

Fig. 8 shows the normal force distribution when the fingertip was pushed at a contact depth of 2 mm. The maximum force area was around the tip close to the nail, with most smaller normal forces distributed near the boundary of the contact surface. This result was similar to the calculation of Tada [10] using a finite element model, as well as to the experimental results on human fingertips illustrated in Fig. 4(a). Thus, although the outer shape of a human fingertip is symmetrical and even, the force distribution is not equal to a hemispherical homogeneous fingertip [3]. The inner distribution of the distal phalanx results in markedly different geometric shapes, as well as non-uniform deformations of beams over the contact area.

Fig. 9 shows the response of friction force during stick to slip phase under constant speed. Similar to the results in Section 3, there were two phases showing a change in frictional force. *Stick phase* represents the pre-slide phase, when the fingertip starts to move but the contact area still sticks to the surface, *i.e.* the entire movement of the fingertip has not yet occurred, during which the frictional force increases. *Slide phase* indicates the total movement of the contact area, with the frictional force remaining constant at constant speed. The smooth change between these two phases is similar to the change in a hemispheric soft fingertip [14]. The friction force varied when some parameters were altered, such as sliding speed and contact depth. As shown in Fig. 9(a), responses of friction force change over time over a wide range of sliding speeds, indicating that stick phase occurs over a small amount of time when the speed increases. Contact depth also affects friction (Fig. 10(a)). At greater contact depth, friction is augmented, and the stick phase elongates over time. This is due to the increase in

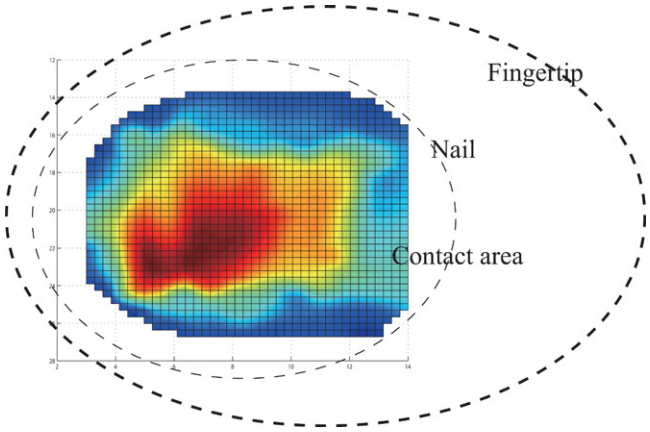

Fig. 8. Normal force distribution on the contact surface in context of fingertip.

normal force when the fingertip is pushed more deeply. We also attempted to change the coefficient of friction, ranging from 0.6 to 2.0, which is typical for human fingertips. As illustrated in Fig. 9(b), the model works well for coefficients of friction larger than 1, indicating that the magnitude of frictional force and the duration of stick phase both increase with fingertips having higher coefficients. Finally, we investigated the dependence of friction on the fineness of the meshed contact area. Fig. 10(b) shows, that for a coarse mesh, friction force is smaller in magnitude, but the duration of stick phase is not altered. This may be due to the coverage ratio of beams over the contact area, as mentioned in Section 4.2. Coverages for coarse and fine mesh were found to be 89% and to 96%, respectively, with the total normal force of coarse case being less than that of fine mesh, resulting in reduced friction.

5.2. Localized Displacement Phenomenon (LDP) during pre-slide phase

One noticeable result of our simulation was its successful representation of localized displacements on the contact area during pre-slide phase. Although several experimental studies measured micro movements on the contact area of human fingertips during sliding [15,16], none could provide an underlying theoretical background for this phenomenon. Using BBM for a hemispheric soft fingertip, we were able to simulate this process, yielding results similar to those described in Section 3.1.

Fig. 11 shows the distribution of localized movements of contacting nodes on the contact area over time during the pre-slide phase. Bright and hot color zones indicate greater movement than cold and dark color zones. These distributions were obtained by simulating a sliding trial at a speed of 2 mm/s, a coefficient of friction of 0.7 and a contact depth of 2 mm. Displacement initially occurred near the boundary of the contact area, gradually propagating in the direction of slide and from outer to inner areas. This propagation of displacement was dependent on normal force distribution, indicating that small forces are distributed mainly near the boundary, not in the middle part (see Fig. 8). Finally, the last area to move right before total slippage of the fingertip happens is circled at time 1.6 s in Fig. 11. This time point is identical to that at which friction starts to be constant in Fig. 9(a), indicating the start of gross slide phase of the fingertip. Experimental evidence [15] has shown that localized slippage occurs first near the boundary area and spreads into the inner zone, with the last area to move being near the tip, a finding similar to the results of our simulation and to the results described in Section 3.1. This phenomenon, while complicated to detect in robotics applications, is easily sensed by the high density of mechanoreceptors underneath the skin in human fingertips. This explains why humans act so comfortably against incipient slippage of a grasped object when it starts to slip out of

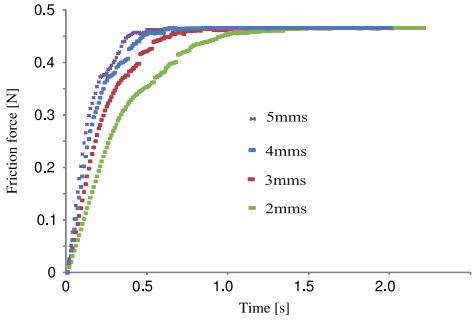

(a) Friction when sliding speed changes.

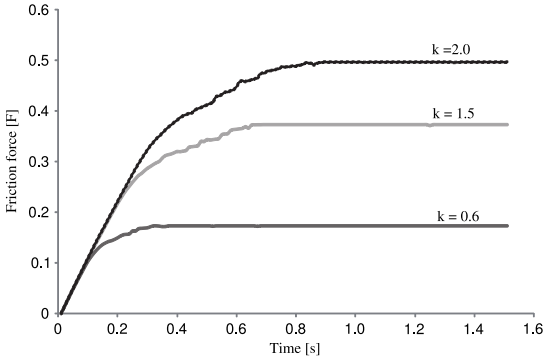

(b) Friction when friction coefficient changes.

Fig. 9. Friction force during stick-to-slide phase.

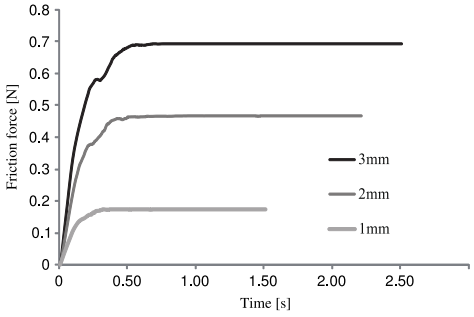

(a) Friction when contact depth changes.

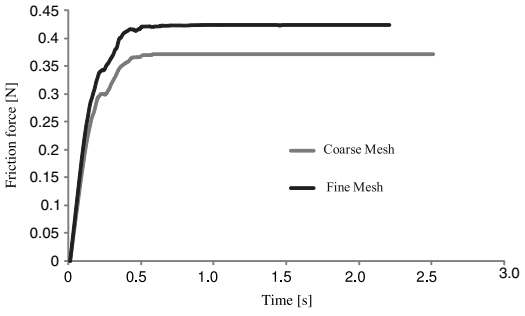

(b) Friction when contact area mesh changes.

Fig. 10. Friction force during stick-to-slide phase.

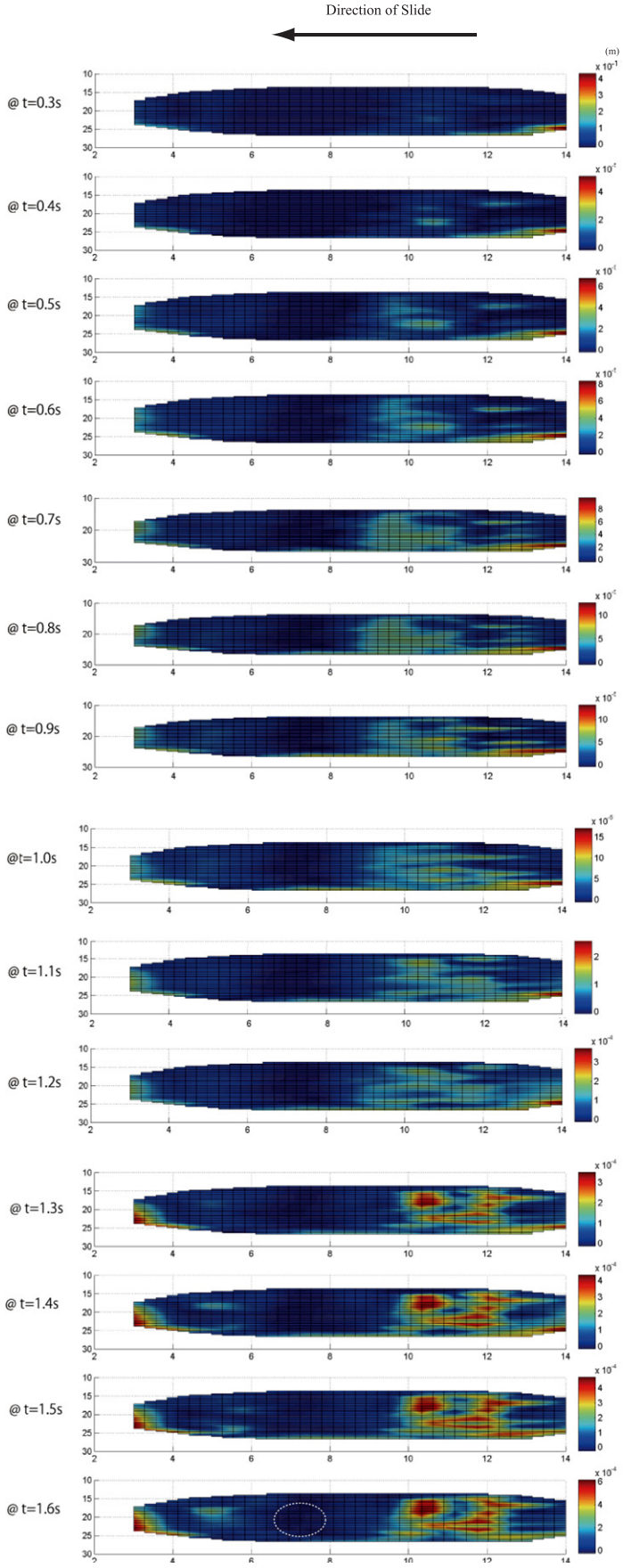

Fig. 11. Localized displacement phenomenon. (For interpretation of the references to color in this figure legend, the reader is referred to the web version of this article.)

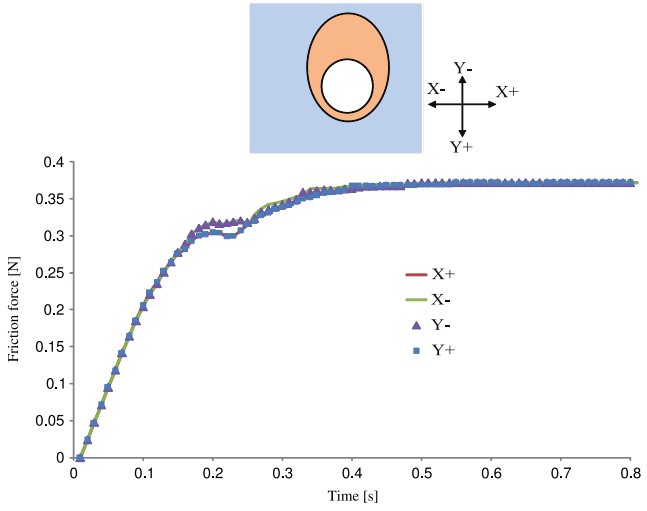

Fig. 12. Frictions over directions of slide.

their hands. Mechanoreceptors do not sense the change of friction force in predicting incipient slippage; rather, they are stimulated by local displacement or stretching of the skin, with tactile signals sent to the brain for processing, and control commands transmitted to the motor system to apply more force to prevent slippage. Thus, by modeling and assessing localized displacement phenomena, we are able to understand the mechanism underlying tactile perception of human fingertips during sliding motion.

The direction of slide was also investigated. For hemispherical fingertips, the friction response and LDP are unchanged, thanks to their symmetry and homogeneity [14]. However, this conclusion is incorrect for human fingertips due to their complicated structure and nonuniform normal force distribution. We conducted simulation trials, in which the fingertip was slid along four directions, $X+$, $X-$, $Y+$, and $Y-$, as illustrated in Fig. 12. Friction responses along the $X+$ and $X-$ (or $Y+$ and $Y-$) directions were almost coincident, with slight differences in friction along the X and Y directions. Thus, change in friction cannot be used to determine friction of slide. Interestingly, however, the profile of LDP is dependent on direction. Fig. 13 shows comparisons of localized displacement distributions on contact areas at several times during pre-slide phase along the $X+$ and $X-$ directions. Differences in propagation of local movements on the contact area were observed between two directions of slide, even on the same axis. A similar phenomenon was observed for the $Y+$ and $Y-$ directions. Although two opposite directions cause different LDPs, as observed in Fig. 13, noticeable differences were observed when the fingertip slid along the X and Y directions. In Fig. 14, we can easily distinguish distinctive propagations of localized movements on the contact surface along two orthogonal directions. Thus, although friction responses are similar when human fingertips slide along different directions, localized displacement phenomena show distinguishable profiles during stick-to-slip phase. These profiles stimulate mechanoreceptors under the skin in different ways, resulting in atypical sensing in various directions. Applying the BBM to modeling human fingertip cannot only assess how and when slippage occurs on a contact area, but can enable understanding of how humans can detect distinguish slippage in a timely manner, based on localized displacement phenomena during stick-to-slip phase. The method by which local slippage erodes the contact area during pre-slide phase can also help to develop sensing systems to sense incipient slippage, as well as to react to prevent it. Simulation results were similar to those observed with a real human fingertip (Section 3), including a two-phase friction response, unsymmetrical normal force distribution, and especially localized displacement during pre-slide phase. Although correct matching between simulated and experimental results are desired, the volunteer who underwent MRI was anonymous and unavailable for validation experiments. Therefore, we have proposed the validation strategy mentioned in the next section.

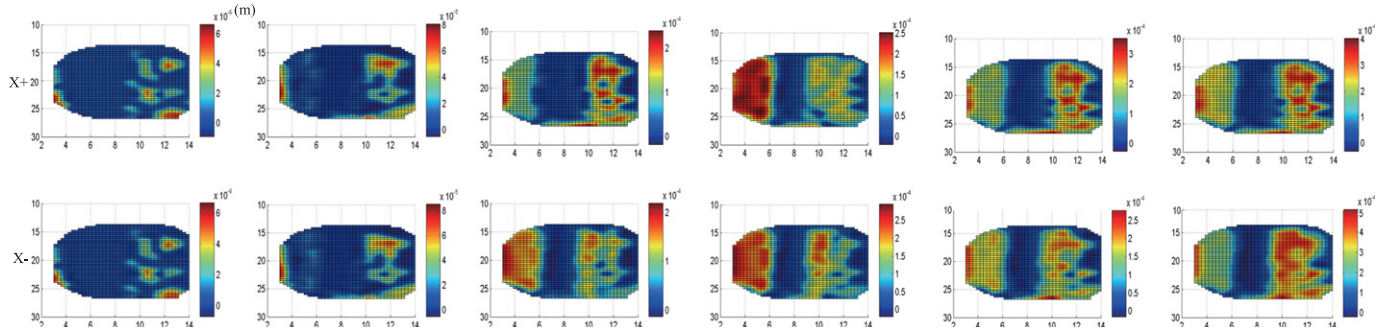

Fig. 13. Comparison in term of local displacement distributions over time when the fingertip slides along $X+$ and $X-$ directions.

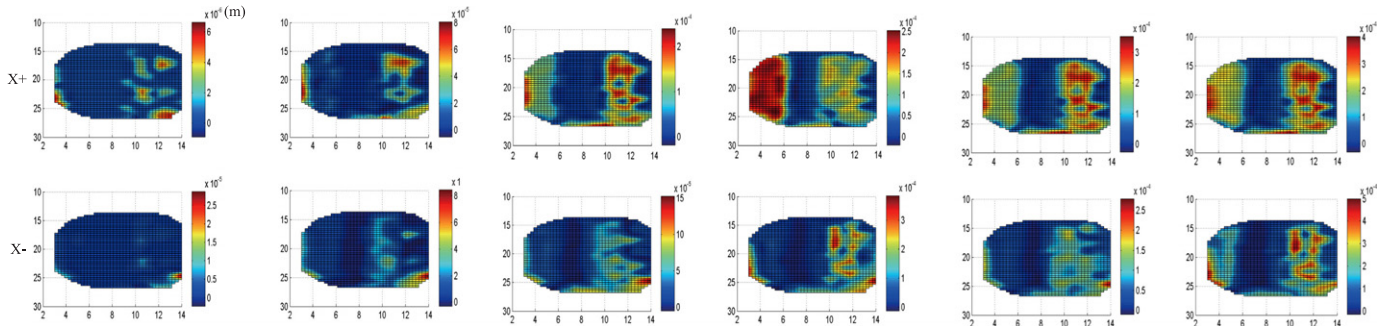

Fig. 14. Comparison in term of local displacement distributions over time when the fingertip slides along $X+$ and $Y+$ directions.

(a) CAD design of the fingertip: soft tissue and bone structure.

(b) Artificial human-like fingertip after curing.

Fig. 15. CAD model of the human-like fingertip.

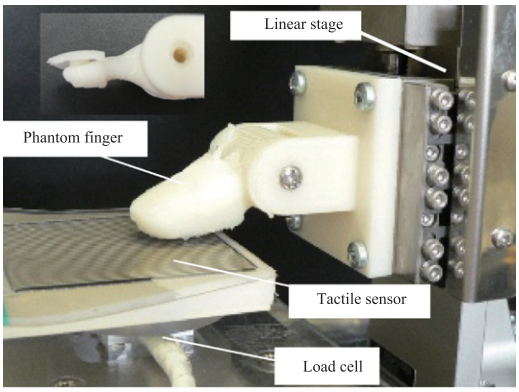

Fig. 16. Experimental setup for validation. Inset picture shows artificially made fingertip structure.

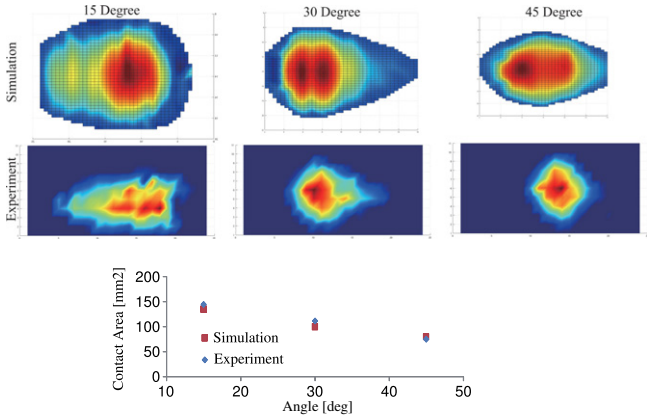

Fig. 17. Comparison of normal force distribution from simulation (upper row) and experiment at different contact angle. The graph shows the relations of contact area and contact angle obtained from simulation and experiment. (For interpretation of the references to color in this figure legend, the reader is referred to the web version of this article.)

5.3. Calculation cost

All codes were implemented in a Microsoft Visual Studio C++ environment, using a common Personal Computer with an Intel Core Duo 3.0 GHz chipset and 2.0 GB RAM. A typical dynamic simulation trial of 2 s took about 24 min to complete. Although not useful for real-time applications, faster performance can be implemented in a GPU-equipped computer. Nevertheless, this computation cost still outperformed typical FE simulations of three-dimensional fingertip models. A similar analysis using ANSYS software was implemented in our previous work [3], but took six to seven hours to complete, and another simulation [13] required several days for each trial. Our method, therefore, is more promising for future real-time applications.

6. Experimental validation strategy

Based on MRI results, we created an artificial inhomogeneous human-like fingertip, with surfaces interpolated and smoothened by a CAD program (see Fig. 15). The bone structure and nail were made by a 3-D printer, while the soft tissue, similar to that of human soft tissue, was made by curing polyurethane rubber gel in a designed mold. Utilizing this finger, we were able to precisely validate the proposed model. To create fingertip movements, we attached it onto a 2-D linear motorized stage that can provide 2 μm-in-resolution step. The fingertip was pushed and slid along a flat rigid plate, fixed to a table with a 3-D loadcell (to measure the three components of force) and a tactile arrayed sensor sheet (for normal force distribution on the contact area) (Fig. 16). To assess localized displacements of the fingertip on the contact area, we marked the skin of the fingertip with black dots distributed similarly to the nodes in the model. These dots were then tracked by a high speed camera during stick-to-slip transition, enabling evaluation of localized displacement phenomena. Using this experimental setup, we were able to vary conditions of contact, such as the angle of contact or direction of slide. Simulations with the artificial fingertip were performed exactly as described in Section 5.2.

6.1. Force validation

6.1.1. Normal force distribution on the contact area

The artificial and CAD fingertips were designed to make normal contact with the surface at three angles of inclination, 15°, 30°, and 45°. The total normal force, measured by the loadcell, was kept unchanged around 1.7 N throughout this validation. In the experiment, the tactile arrayed sensor recorded distributions of normal force, and the data were compared with simulation results. Fig. 17 shows agreement between the simulation and experimental results. Both showed similar linear relationships between the contact area and angle of inclination, as illustrated in Section 3.2. Thus, the proposed method can predict detail normal distribution. The inclusion of bone structure results in a force distribution different from that observed with a homogeneous robotic fingertip.

6.1.2. Friction response

In this validation, we attempted to compare responses of friction during sliding motion under various conditions of contact, resulted from simulations and experiments on artificial fingertips.

Figs. 18–19 show the agreement between simulation and experimental results at two contact angles, 15° and 45°. The error was significant only at the initial time point, declining to less than 10% during the transition. The difference was due to an artifact of numerical simulation. The simulated and experimental results both verified the occurrence of a stick phase prior to gross sliding of the fingertip, during which friction increases significantly and almost linearly. The graphs in Fig. 20 indicate that decreasing the angle of inclination at contact, while maintaining the same contact

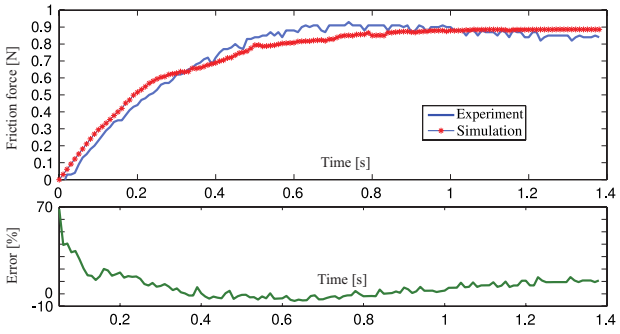

Fig. 18. Comparison of friction responses in simulation and experiment at $\theta = 15°$, and $v = 6$ mm/s.

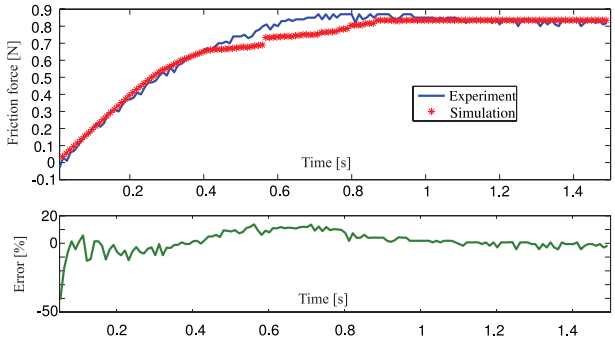

Fig. 19. Comparison of friction responses in simulation and experiment at $\theta = 45°$, and $v = 5$ mm/s.

depth and sliding velocity, increases the duration of the stick phase. Similar findings were observed experimentally. When angle of contact is low, the contact area is wider, requiring more time for localized displacement to occur; moreover, friction is greater at the same contact depth and sliding speed. We also assessed whether friction response was altered when the direction of fingertip movement was changed. The simulation and experimental results shown in Fig. 21 illustrates that friction did not vary significantly when the fingertip was moved over four directions. Friction was always slightly greater along the $Y+$ direction than along the other directions, similar to the results shown in Section 5.1. This finding indicates that these slight differences are insufficient for humans to feel, making it difficult to determine direction of slide based on friction alone.

6.1.3. Localized displacement phenomenon

To verify this phenomenon, we mimicked the method employed for the human fingertip in Section 3.1 by marking a net of black dots on the outer skin of the artificial fingertip (Fig. 15) and sliding the fingertip along the X and Y directions. Figs. 22 and 23 illustrate partial movements of contacting areas in the contact pad during the pre-slide phase, obtained from both simulations and experiments, in the two directions. The movements of contacting points in the experiments are indicated by white bars, determined using the optical tracking method [15]. The hot colors observed in the simulation represent larger displacement areas on the contact pad (note that the color scale differs over images). The simulated and experimentally determined propagation of slippage on the contact pad were similar. Boundary areas, in which the normal force distributions are smaller according to Fig. 17, slipped before the propagation started to erode the inner areas. Moreover, the propagation of localized slippage varied significantly when the fingertip was slid along different directions, similar to findings in Section 5.2. This, again, supports our hypothesis, that skin stretching caused by localized displacement is the main stimulus by which mechanoreceptors underneath the skin of human fingertips feel tactile sensations regarding sliding action. These findings verify the use of BBM in an artificial human-like fingertip with a fine experimental setup. Most of the mechanical characteristics of sliding of the artificial fingertip were similar to those of the simulation, such as friction and the localized displacement phenomenon.

6.1.4. Localized displacement phenomenon

To verify this phenomenon, we mimicked the method employed for the human fingertip in Section 3.1 by marking a net of black dots on the outer skin of the artificial fingertip (Fig. 15) and sliding the fingertip along the X and Y directions. Figs. 22 and 23 illustrate partial movements of contacting areas in the contact pad during the pre-slide phase, obtained from both simulations and experiments, in the two directions. The movements of contacting points in the experiments are indicated by white bars, determined using the optical tracking method [15]. However, the hot colors observed in the simulation represent larger displacement areas on the contact pad (note that the color scale differs over images). The simulated and experimentally determined propagation of slippage on the contact pad were similar. Boundary areas, in which the normal force distributions are smaller according to Fig. 17, slipped before the propagation started to erode the inner areas. Moreover, the propagation of localized slippage varied significantly when the fingertip was slid along different directions, similar to findings in Section 5.2. This, again, supports our hypothesis, that skin stretching caused by localized displacement is the main stimulus by which mechanoreceptors underneath the skin of human fingertips feel tactile sensations regarding sliding action. These findings verify the use of BBM in an artificial human-like fingertip with a fine experimental setup. Most of the mechanical characteristics of sliding of the artificial fingertip were similar to those of the simulation, such as friction and the localized displacement phenomenon.

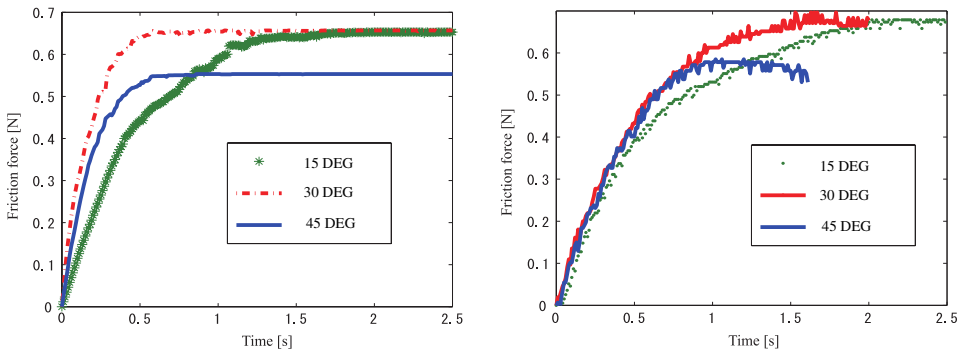

(a) Simulation. (b) Experiment.

Fig. 20. Comparison of friction responses in simulation and experiment when the contact angle varies.

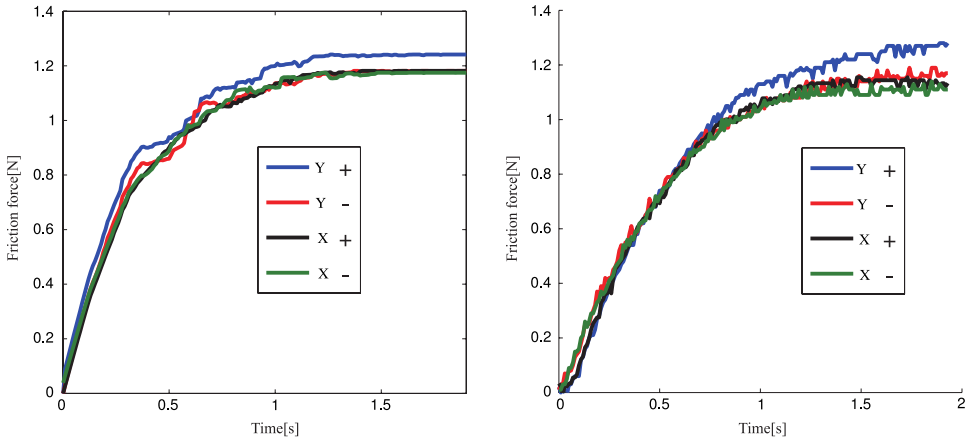

(a) Simulation. (b) Experiment.

Fig. 21. Friction response when the fingertip slides over four directions as illustrated in Fig. 12.

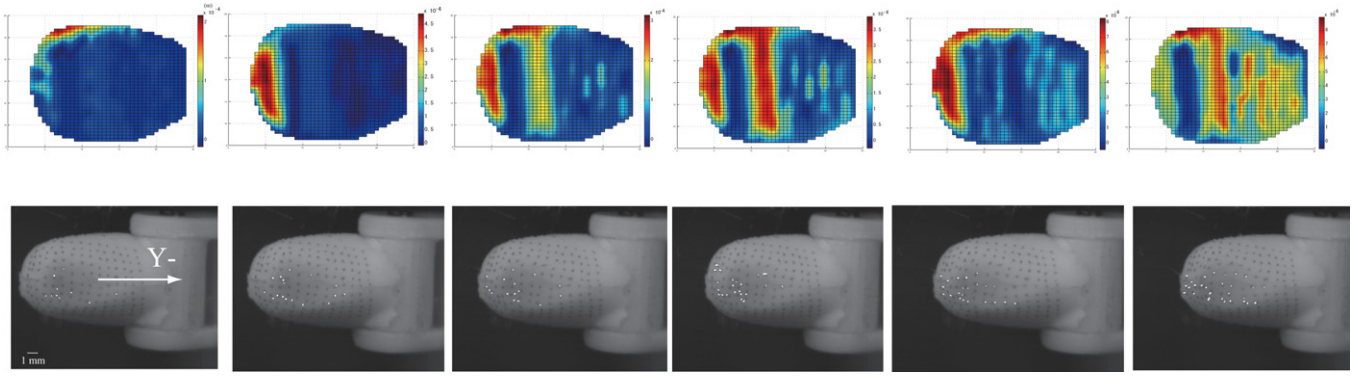

Fig. 22. Comparison in term of local displacement distributions over time when the fingertip slides along $Y-$ directions. Upper row is results from simulation.

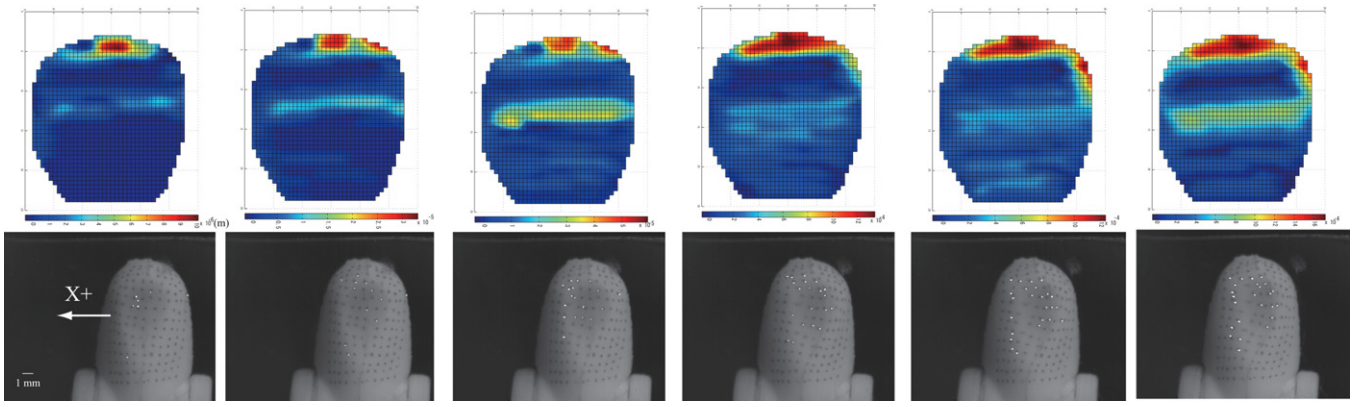

Fig. 23. Comparison in term of local displacement distributions over time when the fingertip slides along $X-$ directions. Upper row is results from simulation.

7. Case study: stable lifting of an object

This section describes the use of the proposed model to simulate the process of lifting an object by two human fingertips, taking into account the change of the localized displacement phenomenon as an input. Humans attempting to lift an object of unknown weight require much less effort than robots, due to the numbers of mechanoreceptors in the fingertips that can detect vibrations stimulated by slippages. Thus humans can slightly increase grip force to stably lift the object, without harming it by hard gripping. Skin stretching causes localized slippage at contact with the object, stimulates mechanoreceptors [19]. Thus, mimicking this process using the proposed model and a simple PD (Proportion-Derivative) control can expedite further theoretical investigations.

7.1. Scenario

In this scenario, two identical human fingertips approached an object of unknown weight. Assuming for simplicity that this object was a homogeneous rectangular cube, visual evaluation may enable individuals to estimate where to grip the object, such that the two fingers would be placed symmetrically on the cube's facets to eliminate any unexpected rotation (see Fig. 24(a)). Nonetheless, humans cannot estimate the exact weight or fragility of an object

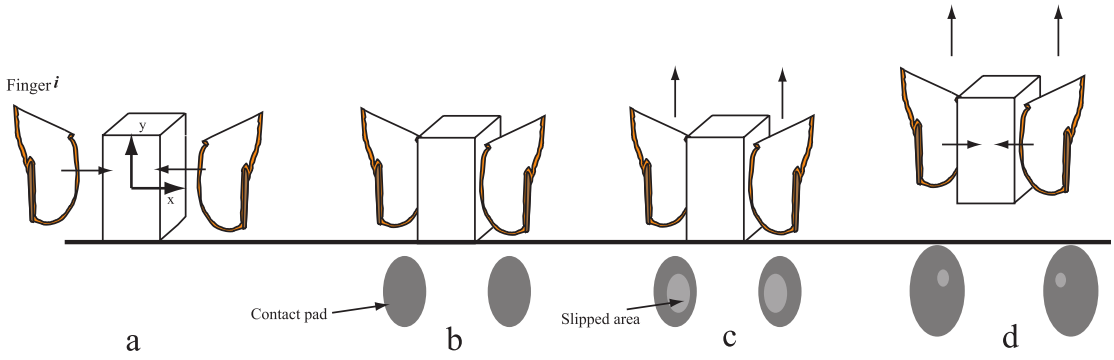

Fig. 24. Stable lifting process of human fingers.

in generating suitable grip force. Therefore, the individual would simply pinch the object with two fingertips in this scenario at the fair initial contact depth (Fig. 24(b)), followed by movement of the two fingertips at low velocity. During this phase, if the slippage zone (dark color in Fig. 24(c)) on the contact pad widened rapidly, *i.e.* the object would be likely to drop. Localized displacements on the contact pad would result in mechanoreceptors beneath the skin sending an about-to-slip signal to the individual's brain. The latter, in return, would sufficiently increase grip force to reduce the slipped area and enhance friction, thus assuring that the object would not slip while being lifted (Fig. 24(d)).

7.2. Quantifying slippage

To evaluate the magnitude of slippage on the contact pad, we introduced a quantitative parameter, called *slip indicator* λ, which was computed based on the ratio between the slipped and contact areas:

$$\lambda = \frac{S_s}{S_c}. \tag{10}$$

This parameter ranges from 0, representing complete sticking, to 1, representing complete slippage state. During incipient slippage, or pre-slide phase, this ratio varies from 0 to 1. Thus, this parameter can represent the current stick/slip state of a contact area between a fingertip and a facet of the object. However, this ratio does not have to be 0 or 1 to result in sticking or slippage, respectively. A small slippage can be acceptable for safe lifting, whereas a rapid increase in this ratio, even to less than 1, can cause slippage. In this simulation, we chose $\lambda_{\text{stick}} = 0.1$ as the largest value for stick phase and $\lambda_{\text{slip}} = 0.5$ as the smallest value for slip phase. These were also two important values for the control of stable objects while simulating lifting.

7.3. Control method

Fig. 25 shows a flowchart for simulation of stable lifting. Two fingers gripped the object at a pre-determined contact depth u_0, and gradually began to move upward. During this phase, the object does not move since the friction generated on contacts with the fingers was smaller than the force of gravity on the object. As shown in the previous sections, the two fingers start to deform, with localized displacements at the contact areas. If the total friction ($f_{\text{fric}} = \sum f^i_{\text{fric}}, i = 1, 2$) is less than gravitational force on the object P_{obj}, and the slip indicator of each finger λ^i is greater than λ_{slip}, say $\lambda^i > \lambda_{\text{slip}}$ ($i = 1, 2$), the two fingers are likely to slip on the object's facets. Thus, a PD control must be introduced to rapidly increase grip force and prevent slippage. Finally, when the total friction is larger than the force of gravity on the object and the slip indicator falls to λ_{stick}, the object can be lifted safely with minimum grip force. In reality, since the force of gravity on an object is unknown, only the condition regarding slip indicator is necessary.

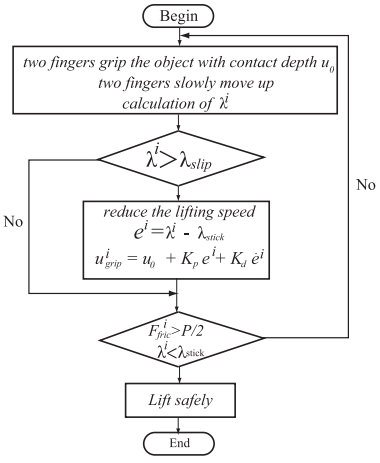

Fig. 25. Control flowchart.

7.4. Simulation result

In this simulation, the object's weight was 120 g (1.2 N) and the coefficient of friction between the fingers and the object's facets was 0.6. For the PD control, $K_p = 3.0$ and $K_d = 1.0$. The initial contact depth u_0 was assigned to 0.8 mm. The speed of fingers was initially increased gradually. When slip was about to occur, the speed was decreased to reduce the possibility of a sudden drop until the stable grip was assured by the PD control. Fig. 26 shows plots obtained during the stable lifting process of human fingertips. First, the two fingertips started to move upward at the initial contact depth u_0, with the object position remaining unchanged. During this phase, the friction generated at one fingertip gradually increased, whereas the localized displacement on the contact area, indicated by the slip indicator λ, increased (see Fig. 26(b)). When 50% of the contact area had slipped, *i.e.*, the fingertips were likely to slip out of the object's facets, the stable gripping control was activated. The contact depths of the two fingertips were increased simultaneously, resulting in a sudden increase in friction as well as a rapid decrease in the slip indicator, assuring that the two fingers did not slide on the object's facets. The PD-control law ensured that the slip indicator was around $\lambda_{\text{stick}} = 0.1$, *i.e.* the object could be lifted safely with minimum gripping force. Using this paradigm, we added another condition, that total friction must be greater than the force of gravity on the object 1.2 N, *i.e.* each finger's friction is over 0.6 N (see Fig. 26), before the object could be lifted safely. The results showed the potential of our proposed model to assess stable grip/grasp mechanism of human soft-fingered hands. Moreover, by evaluating localized displacement on the contact area, a stable grasp/manipulation can be assured with minimum grip force from human fingers. Further investigations based on our model can

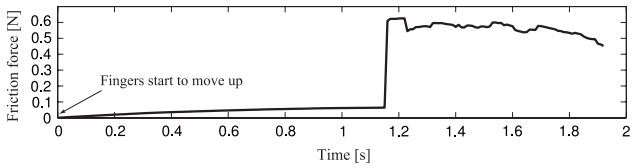

(a) Friction force of one fingertip.

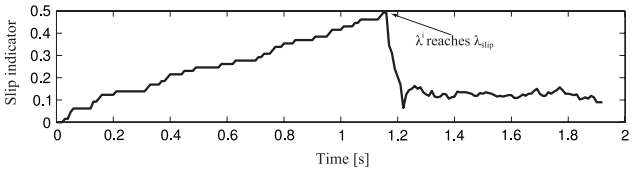

(b) Slip indicator of one fingertip.

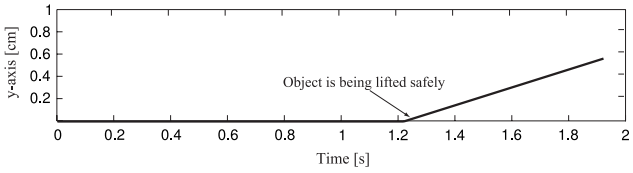

(c) Gripped object position along *y*-direction.

Fig. 26. Simulation result during the stable lifting.

include the lifting of irregular objects and the stabilization of grasped objects during disturbances.

8. Discussion

8.1. Significance of the LDP in tactile sensing

Touching/sliding action of human fingertips on smart devices is a new type of contact. Interactions between human fingertips and machines require a novel sensing system that can detect various actions, such as pushing, squeezing, and especially sliding. Nonetheless, detection of incipient slippage of human and soft robotic fingertips is challenging due to the unpredictability of sticking/slipping before gross sliding. Our proposed BBM suggested a way to model inhomogeneous soft fingertips in order to determine *how* and *when* slippage occurs during the stick phase through the propagation of *localized displacements* on the contact area. This may help intuitively image the phenomenon that dominates during sliding contact. In tactile sensing, humans do not feel the exact frictional force acting on a contact area. Rather, mechanoreceptors beneath the skin are stimulated by *skin deformation/stretching* through stress or vibration, with signals transferred to the brainstem along the axonal process [19], allowing tactile sensations to be interpreted. This supports our idea of utilizing the LDP in detecting incipient slippage with a tactile sensing system. If a sensing system can detect the propagation of slippage on a contact area during the stick phase, either *directly* or *indirectly*, the incipient slippage can be judged properly and in a *timely* manner. One direct method is to use a high speed camera to track movements at each contact point, showing where the contact patch does and does not slide. Due to its size, however, this method is not suitable for embedding in any system. Therefore, a novel, easy to fabricate, sensing system must be utilized to indirectly conform to the LDP. This indirect method must account for localized displacements in its transduced output, so that robots/machines can assess whether slippage is about to occur.

8.2. Beam Bundle Model

We have shown a process for application of the BBM in modeling various types of human-like fingertips, from actual to artificially designed and from homogeneous to inhomogeneous fingertips. The main characteristics of sliding human fingertips were successfully incorporated into the simulated model, especially the localized displacements during the pre-slide phase. This can act as a platform for studying sliding mechanics of robotic fingertips in tactile perception, or creating models in a virtual environment for haptic research. The geometric structure of fingertips indicates that this model is applicable for modeling their sliding action. In this research, tissue volume was modeled with an elastic element (virtual beams), and the skin layer (contact area) as a visco-elastic (Voigt) element. Actual human tissue, however, is more complicated, making the elastic model insufficient. More complicated models can be used for beams, such as a Voigt model. If a beam consists of n Voigt elements, ε would be the extensional strain of the beam and ε_i would be the extensional strain of the ith element. Extensions ε and ε_i through ε_{n-1} are independent state variables, and ε_n can be described dependently by other variables:

$$\varepsilon_n = \varepsilon - \varepsilon_1 - \cdots - \varepsilon_{n-1}. \tag{11}$$

Let E_i and c_i be the elastic and viscous moduli of the ith Voigt element. Since stresses generated by individual elements are equal to each other, then:

$$\sigma = E_1\varepsilon_1 + c_1\dot{\varepsilon_1} = E_2\varepsilon_2 + c_2\dot{\varepsilon_2} \cdots = E_n\varepsilon_n + c_n\dot{\varepsilon}, \tag{12}$$

where σ indicates the stress generated by the deformation of the beam. Dividing the above equations by c_1 through c_n and summing up all equations yields:

$$\sigma = \frac{\left(\frac{E_1}{c_1}\varepsilon_1 + \cdots + \frac{E_{n-1}}{c_{n-1}}\varepsilon_{n-1}\right) + \frac{E_n}{c_n}(\varepsilon - \varepsilon_1 - \cdots \varepsilon_{n-1}) + \dot{\varepsilon}}{\frac{1}{c_1} + \frac{1}{c_2} + \cdots \frac{1}{c_n}}. \tag{13}$$

Note that, using the above equation, stress σ can be computed from state variables ε_1 through ε_{n-1} and $\dot{\varepsilon}$. These state variables satisfy the following differential equations:

$$\dot{\varepsilon_1} = -\frac{E_1}{c_1}\varepsilon_1 + \frac{1}{c_1}\sigma, \ldots, \dot{\varepsilon}_{n-1} = -\frac{E_{n-1}}{c_{n-1}}\varepsilon_{n-1} + \frac{1}{c_{n-1}}\sigma. \tag{14}$$

Consequently, a dynamic equation can be utilized to calculate deformations of elements in an inhomogeneous beam. This process was repeated for all virtual beams in a fingertip. This derivation can also be utilized to model any inhomogeneous soft objects other than fingertips. Using this extension, the reaction of normal force during loading/unloading of fingertip can be modeled more realistically. Fig. 27(b) illustrates one simulated dynamic load/unload test of normal force response. Exponential growth and decay of the normal force occurred during the loading and unloading phases, respectively. Also, relaxation of the normal force, when the fingertip was held, was successfully represented in simulation.

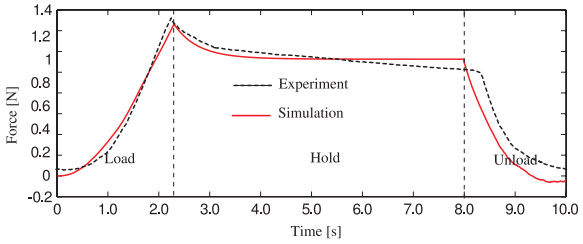

Fig. 27. Graph show a dynamic response of the total normal force during simulated load/unload test.

9. Conclusion

We have theoretically investigated the sliding motion of a human fingertip model, focusing on the pre-slide phase and utilizing the previously proposed BBM and MR images. Simulation results can help assess changes of force, especially localized displacement phenomena, on the contact area during pre-slide phase. This knowledge may assist in understanding the role of skin in recognition of slippage, as well as in the development of a sensing system that can detect incipient slippage of human fingertip, which is crucial for stable manipulation.

References

[1] Mark H. Lee, Tactile sensing: new directions, new challenges, Int. J. Robot. Res. 19 (7) (2000) 636–643.
[2] A. Nahvi, J.M. Hollerback, R. Freier, D.D. Nelson, Display of friction in virtual environments based on human finger pad characteristics, in: Proceedings of ASME Conference.
[3] V.A. Ho, D.V. Dao, S. Sugiyama, S. Hirai, Development and analysis of a sliding tactile soft fingertip embedded with a micro force/moment sensor, IEEE Trans. Robot. 27 (3) (2011) 411–424.
[4] K.J. Astrom, C. Canudas-de-Wit, Revisiting the LuGre friction model, IEEE Control Syst. Mag. (2008) 101–114.
[5] T. Maeno, S. Hiromitsu, T. Kawai, Control of grasping force by detecting stick/slip distribution at the curved surface of an elastic finger, in: IEEE Int. Conf. on Robotics and Autom., San Francisco, May, 2000, pp. 3895–3900.
[6] N. Xydas, M. Bhagavat, I. Kao, Study of soft-finger contact mechanics using finite analysis and experiments, in: IEEE Int. Conf. on Robotics and Automation, Vol. 3, April 2000, pp. 2179–2184.
[7] M.A. Srinivasan, K. Dandekar, An investigation of the mechanics of tactile sense using two-dimensional models of the primate fingertip, Trans. ASME, J. Biomech. Eng. 118 (1996) 48–55.
[8] K. Dandekar, B.I. Raju, M.A. Srinivasan, 3-D finite-element models of human and monkey fingertips to investigate the mechanics of tactile sense, Trans. ASME, J. Biomech. Eng. 125 (2003) 682–691.
[9] S. Shimawaki, N. Sakai, Quasi-static deformation analysis of a human finger using a three-dimensional finite element model constructed from CT images, J. Environ. Eng. 2 (2007) 56–63.
[10] M. Tada, Individual difference in contact, J. Robot. Soc. Japan 30 (5) (2012) 17–19.
[11] I. Kao, M.R. Cutkosky, Quasistatic manipulation with compliance and sliding, Int. J. Robot. Res. 11 (1) (1992) 20–40.
[12] M. Konyo, S. Okamoto, Pseudo haptic representations using vibrotactile stimuli, J. Robot. Soc. Japan 30 (5) (2012) 23–25.
[13] Z.K. Wang, L. Wang, V.A. Ho, S. Morikawa, S. Hirai, A 3D non-homogeneous FE model of human fingertip based on MRI measurements, IEEE Trans. Instrum. Meas. 61 (12) (2012) 3147–4157.
[14] V.A. Ho, S. Hirai, Understanding slip perception of soft fingertips by modeling and simulating stick–slip phenomenon, in: Robotics: Science and Systems VII, Los Angeles, CA, US, June 2011.
[15] M. Tada, T. Kanade, An imaging system of incipient slip for modeling how human perceives slip of a fingertip, in: The 26th Annual Intl. Conf. of the IEEE EMBS, San Francisco, September, 2004, pp. 2045–2048.
[16] M. Tada, T. Shibata, M. Imai, T. Osagawara, Development of the simultaneous measurement system of finger tip deformation and grip/load force for studies of human grasping skill, Trans. Jpn Inst. Electron. Inf. Commun. Eng. D-II 84 (2001) 1033–1044.
[17] J.L. Johnson, Contact Mechanics, Cambridge University Press, 1985, (Chapter 4).
[18] R.D. Mindlin, Compliance of elastic bodies in contact, Trans. ASME J. Appl. Mech. 16 (1949) 259–268.
[19] M.J. Hertenstein, S.J. Weiss, The Handbook of Touch, Springer Publishing Company, New York, 2011.

Van Anh Ho was born in Halong, Vietnam in 1984. He received the B.S. degree in Electrical Engineering, in 2007, from Hanoi University of Technology, and the M.S. and Ph.D. degrees in robotics, in 2012, from Ritsumeikan University, where he is currently working as Japan Society for Promotion of Science (JSPS) Postdoctoral Fellow.

His current research interests include automation engineering, robotics, anthropomorphic hand, soft fingered manipulation, and fabrication of tactile sensor. He is a student member of IEEE, RSJ.

Shinichi Hirai received his B.S., M.S., and Doctoral degrees in applied mathematics and physics from Kyoto University in 1985, 1987, and 1991, respectively. He is currently a Professor in the Department of Robotics at Ritsumeikan University. He was a Visiting Researcher at Massachusetts Institute of Technology in 1989 and was an Assistant Professor at Osaka University from 1990 to 1996. His current research interests are modeling and control of deformable objects, realtime computer vision, and soft-fingered manipulation.

He received SICE (Society of Instrument and Control Engineers) Best Paper Award at 1990, JSME (Japan Society of Mechanical Engineers) Robotics and Mechatronics Div. Achievement Awards at 1996, the finalist of Automation Best Paper Award at 2001 IEEE Int. Conf. on Robotics and Automation, the finalist of Manipulation Best Paper Award at 2005 and 2006 IEEE Int. Conf. on Robotics and Automation, the finalist of Vision Best Paper Award at 2006 IEEE Int. Conf. on Robotics and Automation, and RSJ (Robotics Society of Japan) Best Paper Award at 2008. He is serving as an Associate Editor of IEEE Transactions on Robotics from July 2006. He is a member of IEEE, RSJ, JSME, and SICE.